Laser-excited intershell rotation of finite Coulomb clusters in a dusty plasma

M. Klindworth, A. Melzer, and A. Piel
Institut für Experimentelle und Angewandte Physik, Christian-Albrechts-Universität Kiel, 24098 Kiel, Germany

V. A. Schweigert
Institute of Theoretical and Applied Mechanics, Novosibirsk, 630090, Russia
(Received 8 November 1999)

The dynamical stability of finite two-dimensional clusters of charged micrometer sized particles is studied experimentally in a dusty plasma, where the particles experience a screened interaction. For clusters containing 19 and 20 particles the intershell rotation barrier height is measured quantitatively by applying a well defined torque on the clusters' outer shell by the radiation pressure of two opposing laser beams. Moreover, a complex behavior is found for the 19-particle cluster where structural transitions occur together with the intershell rotation showing that the presence of shielding can basically change the least stable modes in finite clusters. The measured crystal properties have been compared with Monte Carlo simulations. Quantitative agreement is found when nonideal effects are taken into account.

I. INTRODUCTION

Finite Coulomb clusters are two-dimensional (2D) systems of a small number of charged particles confined by an external field. Such cluster configurations have already been analyzed in line with Thomson's classical atom model[1] and since then have been a topic of theoretical studies with respect to particle ordering, phase transitions, eigenmodes, and energy spectra (see, e.g., Refs. 2,3).

Experimentally, Coulomb clusters have been successfully realized in systems with electrons on a liquid helium surface[4] and in quantum dots,[5] or, using macroscopic particles, in colloidal suspensions.[6,7] Recently, Coulomb clusters of charged micrometer sized particles were studied in dusty plasmas by Juan *et al.*,[8] who investigated the structure of clusters with up to several hundred particles.

Since the first observations of Coulomb crystallization in these systems,[9–12] dusty plasmas have been shown to be ideal strongly coupled systems bridging the fields of plasma physics and condensed matter. In those experiments, typically, micrometer sized monodisperse (plastic) particles, the ''dust'' particles, are immersed into a gaseous plasma discharge where the particles become charged by the continuous inflow of plasma electrons and ions. In general, the particles attain a high negative equilibrium charge (of the order of 10^4 elementary charges) due to the much higher velocities of the electrons. The particles are then trapped in the space charge sheath above a lower flat horizontal electrode, where strong electric fields prevail that levitate the negative charges against gravity, quite similarly to Millikan's historic oil drop experiment. Here, however, the electric field is spatially inhomogeneous due to the presence of the free plasma charges, and thus a quite strong vertical confining potential for the particles is formed, forcing the particles to arrange themselves in a horizontal layer. In the horizontal plane the particles are usually confined by ring-shaped disturbances of the sheath electric field.

The dust particles are efficiently held at room temperature by friction with the ambient neutral gas (the fraction of atoms split into electrons and ions forming the plasma is very small). Due to the high particle charges Coulomb crystallization is possible even at room temperature with the particles arranged in ordered structures, the so called plasma crystal.

Whereas the plasma crystals that form in dusty plasmas[9–12] consist of many (10^4 to 10^5) particles, recently experiments on finite Coulomb clusters have been reported.[8] Actually, plasma crystals[9,10,12] can be considered as Coulomb clusters, too. The difference between them is the nonstatistical number of particles of the finite Coulomb cluster and the importance of the cluster boundary conditions given by the particle confining fields.

Recent experiments have shown that dust particle motion can be effectively excited and manipulated by means of a focused laser beam.[13–17] Here, we present experiments on the dynamical stability of these finite clusters. From theoretical studies[3] intershell rotation, which is the differential rotation of two neighboring concentric rings of the cluster, is predicted to be the least stable mode in finite clusters up to about $N=50$ particles. In the experiment, the intershell rotation is directly excited by two opposing laser beams which apply a well defined torque on the cluster. From the reaction of the cluster to this torque the stability of these clusters can be deduced.

II. FINITE COULOMB CLUSTERS

Finite Coulomb clusters consist of two-dimensional arrangements of N charged particles confined in a potential well. The physics of these finite clusters has been widely discussed in the literature,[2,3,18] so here only a short description of the main properties will be given.

In dusty plasmas, the electrostatic interaction between two dust particles can be assumed to be of Debye-Hückel (Yukawa) type, which was verified by recent experiments on dust lattice waves[13,14] and direct collisions of dust grains.[19] The repulsive potential between two particles i,j is thus given by

$$\Phi(r_{ij}) = \frac{Q}{4\pi\epsilon_0 r_{ij}} \exp\left(-\frac{r_{ij}}{\lambda_D}\right), \tag{1}$$

where Q is the particle charge and λ_D the screening length, $\vec{r}_i = (x_i, y_i)$ and $r_{ij} = |\vec{r}_i - \vec{r}_j|$. It is usually assumed that the particles (of mass m) are confined in a parabolic horizontal potential well with the eigenfrequency ω_0,

$$V(\vec{r}_i) = \frac{m\omega_0^2}{2}(x_i^2 + y_i^2). \tag{2}$$

Then the total energy of the cluster with N particles is

$$E_{\text{total}} = \sum_{i=1}^{N} V(\vec{r}_i) + \sum_{j<i}^{N} Q\Phi r_{i,j}. \tag{3}$$

A natural unit of energy in these finite clusters is[2]

$$E_0 = \sqrt[3]{\left[\left(\frac{Q^2}{4\pi\epsilon_0}\right)^2 \frac{m\omega_0^2}{2}\right]}.$$

The force acting on a single particle i then simply reads

$$\begin{aligned}\vec{F}_i &= -\vec{\nabla} E_{\text{total}} \\ &= \vec{F}_{\text{p}}(\vec{r}_i) + \sum_{j=1,\, j\neq i}^{N} \vec{F}_{\text{c}}(\vec{r}_i - \vec{r}_j) \\ &= -m\omega_0^2 \vec{r}_i + \frac{Q^2}{4\pi\epsilon_0} \sum_{j=1,\, j\neq i}^{N} \frac{\vec{r}_i - \vec{r}_j}{r_{ij}^3} \exp\left(-\frac{r_{ij}}{\lambda_{\text{D}}}\right)\left(1 + \frac{r_{ij}}{\lambda_{\text{D}}}\right).\end{aligned} \tag{4}$$

The finite Coulomb clusters are arranged in a structure that minimizes the total energy of the system given by Eq. (3). A Mendeleev table of the cluster structures was presented for pure Coulomb interaction (i.e., $\lambda_D \to \infty$) in Ref. 2 and for shielded interaction in Refs. 20 and 18. It was found that, for small $N < 50$, the particles are arranged in ringlike shells due to the axial symmetry of the confining potential.

From further studies[2,3] the type of motion with the lowest excitation energy in a finite cluster is predicted to be intershell rotation, where two neighboring shells differentially rotate with respect to each other. The threshold for excitation of this mode, however, dramatically depends on the particle number N (and the associated cluster structure). An outstanding example for the number N dependence of the intershell rotation is given by the pair of $N = 19$ with one particle in the center, 6 in the inner shell, and 12 in the outer shell (1,6,12) and $N = 20$ (1,7,12) particles (see also Fig. 1). Here the highly symmetrically arranged $N = 19$ cluster is extremely stable against intershell rotation (which, however, still is the least stable mode), whereas $N = 20$ (1,7,12) is found to be extremely unstable.[3] The reason for the difference in the stability threshold is believed to lie in the sixfold symmetry of the $N = 19$ cluster and the completely broken symmetry of $N = 20$.

This experimental study is mainly restricted to the investigation of clusters with two rings with or without an additional central particle, which are dynamically equivalent, since the central particle carries no angular momentum. A two-ring structure is established between $N = 9$ (2,7) and $N = 21$ (1,7,13). Special attention is paid to the $N = 19,20$ configurations mentioned above.

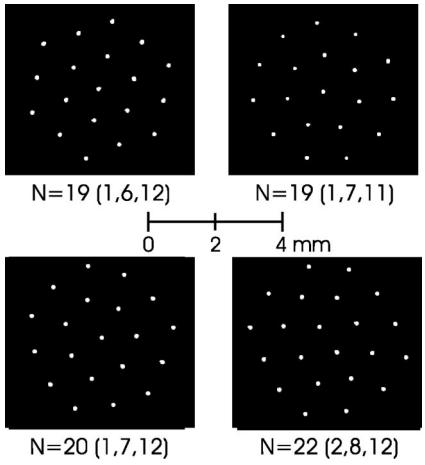

FIG. 1. CCD camera snapshots of the $N = 19$ (1,6,12) and (1,7,11), 20, and 22 clusters in the plasma sheath.

III. EXPERIMENTAL METHOD

The experiments are performed in a radio-frequency discharge between two large horizontal electrodes (of 17 cm diameter) at 13.56 MHz in helium at gas pressures ranging from 15 to 30 Pa. The upper electrode is realized as a grounded grid to ensure observation of the dust particles from the top, while the lower one is powered at about 9–12 W and a rf voltage of $35 V_{pp}$ (V_{pp} is the peak-to-peak voltage). The dust grains used in the experiment are monodisperse spherical plastic particles of $d = (9.47 \pm 0.3)$ μm diameter and of mass $m = 6.73 \times 10^{-13}$ kg. The particles are injected by a dust dropper above the upper electrode. The dust dropper is a dust particle container with an extremely small hole (300 μm diameter) in the bottom. By weakly shaking the dropper from outside particles fall through the hole, which allows the injection of a small number of dust particles only. The particles are trapped in a horizontal plane in the sheath boundary above the lower electrode, where the electric field force $QE(z_0)$ balances the force of gravitation mg (z denotes the vertical height of the particles above the electrode). With the spatially inhomogeneous electric field $E(z) = E(z_0) + E'(z - z_0)$ this results in a very strong *vertical* confinement potential $V(z) = QE'(z - z_0)^2/2$. The grains are illuminated by a horizontally expanded sheet of HeNe laser light (at 632 nm) and the scattered light is recorded with a charge-coupled device (CCD) video camera from the top (see Fig. 2).

To create a parabolic potential well $V(r)$ to confine the particles *horizontally*, a metal plate of 5 cm diameter with a spherical trough of 2 mm depth and 15 cm radius of curvature is placed on top of the lower electrode (see Fig. 3). The electrostatic equipotential lines in the sheath are assumed to follow this trough, providing the horizontal confinement.

To excite the intershell rotation in a cluster, the beam of a laser diode at 690 nm wavelength is focused on one or two particles in the outer ring. The laser light is then reflected and focused again on the outer ring, but on the opposite side. The radiation pressure of the beam therefore generates a

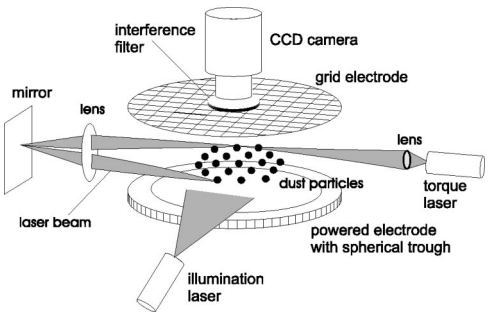

FIG. 2. Schematic view of the experimental setup.

symmetric pair of forces that exerts a torque on the outer ring of the cluster, leading to the rotation of the outer ring. The strength of the torque can be changed by varying the laser power. The inner ring is then found rotating under the influence of forces due to the intershell rotation barrier and the opposing friction with the neutral gas. For observation of the cluster with the CCD camera the light of the torque laser is suppressed by an interference filter tuned to pass the illuminating HeNe laser light. For further analysis the video sequences of several minutes are digitized by a frame-grabber card and processed by a PC.

IV. RESULTS

A. Dust and plasma parameters

The dust particle charge is measured by the *vertical* oscillation resonance method.[12,21] There, vertical oscillations of the trapped particles in the vertical potential well $V(z)$ are excited by modulating a low-frequency (between 1 and 100 Hz) sinusoidal voltage onto the rf voltage. From the vertical resonance frequency ω_{res}, the dust charge can be derived from

$$V(z)=\tfrac{1}{2}QE'(z-z_0)^2=\tfrac{1}{2}m\omega_{\mathrm{res}}^2(z-z_0)^2.$$

The dust charge is determined as $Q=12\,100e$ at the plasma conditions mostly used (9 W, 21 Pa).

The eigenfrequency ω_0 of the *horizontal* confinement potential $V(r)$ due to the curved electrode is determined in a similar way by exciting horizontal oscillations of one or several particles by a periodic voltage applied to a tungsten wire in the plasma sheath close to the particles.[22–25] From the resonance curve for the oscillations the horizontal eigenfrequency is determined as $\omega_0=2\pi\times1.3\ \mathrm{s}^{-1}$. From the width of the resonance the dust–neutral gas friction coefficient is

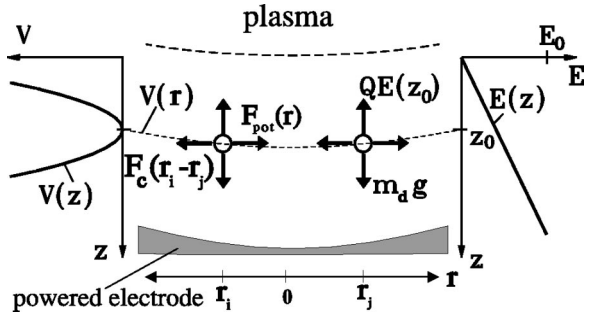

FIG. 3. The effective forces and fields balancing the dust particles in the plasma space charge sheath.

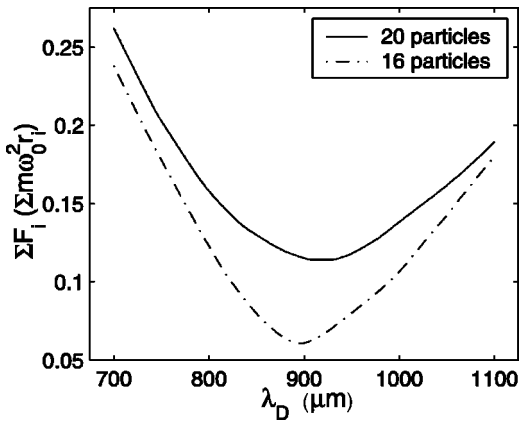

FIG. 4. Sum of all forces on $N=16$ and $N=20$ clusters as a function of the screening length (normalized to the potential forces).

measured as $\nu=5.5\ \mathrm{s}^{-1}$, which is in good agreement with the theoretical Epstein coefficient.

Knowing Q and ω_0, the screening length λ_D can be evaluated from the measured particle positions $\vec{r}_i$ in the clusters. Therefore, the forces on the particles are summed and that value of λ_D that minimizes the residual sum $|\Sigma_{i=1}^{N}\vec{F}_i|$ [according to Eq. (4)] is taken as the shielding length. Figure 4 shows the residual forces of two particle constellations as a function of λ_D. The value of $\lambda_D=900\ \mu$m is in good agreement with previous work[22,13] and results in a screening strength $\kappa=a/\lambda_D=1.1$ with an average particle distance $a=1000\ \mu$m. With the eigenfrequency of the horizontal confinement potential, the charge of the particles, and the screening length, the energies in the cluster can be evaluated.

When a torque is applied to a shell-structured cluster, there is a difference in angular velocity between the laser driven outer shell and the inner shell, which is slowed down by gas friction. The force that the outer shell exerts on the inner shell can be determined from an analysis of the two rotation velocities and the particles' radial and angular coordinates. Finally, the height of the intershell energy barrier can be estimated.

B. Clusters without laser torque

First, experiments on the finite clusters without laser torque will be investigated with regard to their stability. The particle arrangement in these clusters coincides with the theoretical predictions of Ref. 2 and the experimental observations of Ref. 8. However, for the $N=19$ cluster the first (meta)stable configuration (1,7,11) was also frequently observed (see Fig. 1).

Without laser drive the clusters rotate very slowly as a whole, presumably due to a weak gas flow in the discharge. The relative motion between the dust grains depends on the number of particles in the cluster. Figure 5 shows typical particle trajectories for $N=19$, 20, and 22 particles, respectively. In the left column, the trajectories of all particles for a duration of 220 s are presented, demonstrating the rotation of the entire cluster. In the right column the relative motion of the particles is shown, by subtracting the overall cluster rotation, taking one of the particles as the reference frame (this can be identified by its trajectory appearing as a radial line

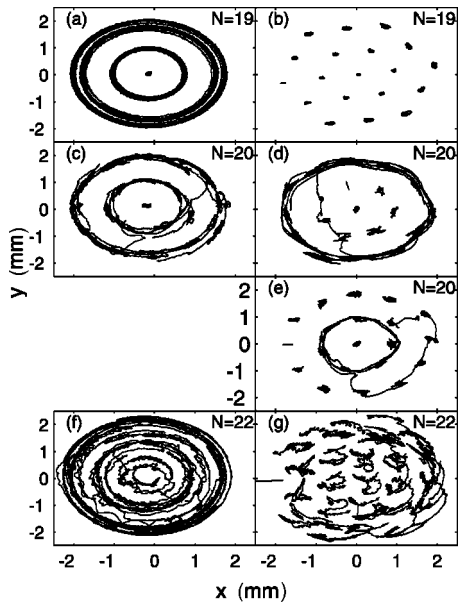

FIG. 5. Dust particle trajectories over 220 s for (a) 19, (c) 20, and (f) 22 particles without laser excitation. (b), (d), (e), and (g) are the trajectories corrected for the cluster rotation.

only). This analysis shows that the 19-particle cluster maintains its highly ordered hexagonal structure and the cluster indeed rotates as a whole. Only weak displacements from the ideal particle positions are observed.

In comparison, the 20-particle cluster shows a decoupling of the outer and inner rings. This becomes evident from the fact that the relative positions in the inner ring, in which the reference particle is chosen in Fig. 5(d), are preserved, whereas the outer ring rotates with respect to the inner one. This kind of motion is interpreted as an intershell rotation. The intershell rotation of two rigid ring systems becomes more evident when, in the same analysis, the reference particle is chosen in the outer ring [Fig. 5(e)], where now the inner ring rotates with respect to the stationary outer one. Moreover, a more complex, vortexlike cluster excitation becomes visible, where one particle changes from the inner to the outer shell, pushing another one from the outer to the inner shell. In contrast to this behavior, the 22-particle cluster does not show ordering within individual rings. It is governed by a mixture of intra- and intershell oscillations and many radial particle exchanges.

The distinct differences between the behavior of 19- and 20-particle clusters will be the focus of the following investigations.

C. Clusters under laser torque

In this section the behavior of the finite clusters for $N=19$ and $N=20$ is described when the intershell rotation is intentionally excited by applying a laser torque.

Figure 6 compares the relative angular velocity $\Delta\varphi/\Delta t$ between outer and inner shell for a 19- and a 20-particle cluster as a function of applied laser power (i.e., laser torque). At low laser torque the relative velocity in the clusters is essentially zero. The clusters rotate as a solid structure. With increasing laser torque the intershell rotation speed increases. It is seen that the intershell rotation is much

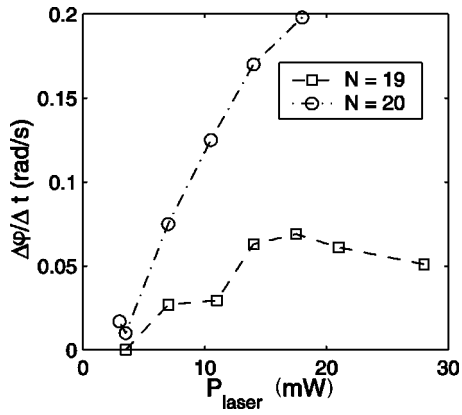

FIG. 6. Average angular velocity difference $\partial\varphi/\partial t$ of outer and inner shell versus laser power for $N=19$ and $N=20$ clusters.

easier to excite for the $N=20$ particle cluster than for $N=19$. It should be noted that, for the $N=19$ cluster, the curve reflects not only the intershell rotation but also structural changes, which are described below.

The temporal behavior of the two clusters will now be investigated in more detail. Figure 7 shows the angular position θ of all $N=19$ (a) and $N=20$ (b) particles as a function of time under almost the same laser torque. The slope of θ vs t is, of course, the angular velocity of a particle. Curves with identical behavior belong to particles of the same shell. In addition, the number of particles in the inner shell is also given.

The $N=20$ cluster [Fig. 7(b)] shows a strong difference in the angular speed of the outer ring (with the larger slope) compared to that of the inner ring, which rotates much more slowly. The rotation speed of the outer ring is very close to constant. For the inner ring a slight modulation of the rotation speed is observable, which hints at some small nonideality in the cluster. The total angular difference between outer and inner ring amounts to about 31 rad, which means that the outer ring exhibits approximately 5 complete revolutions with respect to the inner ring. Finally, the number of particles in the inner shell (and thus in the outer shell, too) is constant at $N_1=7$.

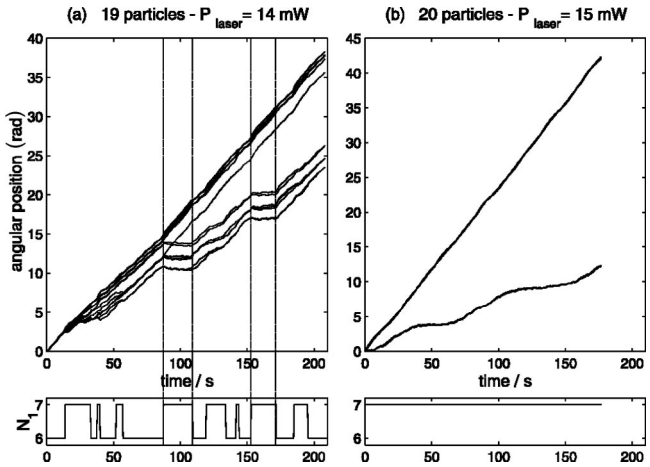

FIG. 7. Relative angular position of the particles in the cluster and number of particles N_1 of the inner shell for (a) 19 particles and (b) 20 particles.

The $N=19$ cluster [Fig. 7(a)] shows a more complex behavior. First, one should note that the structure of the cluster is changing between (1,6,12) and (1,7,11), as seen from the behavior of N_1 over time. From the angular position as a function of time one can identify two regimes. In the first, all particles move with the same velocity (same slope for all particles) which corresponds to a rotation of the cluster as a whole. In the second regime, the particles of the inner ring show constant angular positions, which means that the inner ring comes to a halt, whereas the outer ring is still rotating. Comparing the structural information and the angular positions, it is found that the cluster is always rotating as a whole when it is in the hexagonal (1,6,12) structure, whereas intershell rotation is only observed for the (1,7,11) structure.

The two alternating constellations of the $N=19$ cluster are investigated in more detail in Sec. V.

D. The intershell interaction energy barrier

From these experiments the intershell rotation energy will be derived and compared with theoretical predictions. Therefore the equation of motion of the dust particles in the cluster has to be analyzed. The particles in the cluster are arranged in two rings of radius $R_{1,2}$ with $N_{1,2}$ particles of mass m in each ring (as mentioned above, the central particle carries no angular momentum and can thus be neglected). The moment of inertia of ring n then simply is

$$I_n = mN_nR_n^2.$$

Then one finds the following equation of motion for the inner ring:

$$I_1\frac{\partial^2\theta_1}{\partial t^2} = \frac{\partial U}{\partial \varphi} - \nu I_1\frac{\partial \theta_1}{\partial t}, \tag{5}$$

where the second term on the right-hand side describes the damping by the neutral gas. A possible approximation of the potential energy of intershell interaction is[3]

$$U = \frac{1}{2}U_\star\left[1-\cos\left(2\pi\frac{\varphi}{\varphi_\star}\right)\right]. \tag{6}$$

Here $U_\star$ is the barrier height, $\varphi_\star$ describes the periodicity of the the intershell barrier, and $\varphi=\theta_2-\theta_1$, where $\theta_{1,2}$ denote the angular positions of the two rings.

In the case of a constant φ, which means no intershell rotation, Eq. (5) reduces to the simpler form

$$\nu I_1\frac{\partial\theta_1}{\partial t} = U_\star\frac{\pi}{\varphi_\star}\sin\left(2\pi\frac{\varphi}{\varphi_\star}\right), \tag{7}$$

from which $U_\star$ can easily be calculated. We can estimate the intershell barrier from the following values: $\nu=5.5\ \mathrm{s}^{-1}$ at 21 Pa. From the simulations (described in Sec. V) $\varphi_\star$ is found to be $2\pi/12$ for a cluster with 12 particles in the outer ring and $\partial\theta_1/\partial t$ is determined from the experimental curve in Fig. 8(a). A constant angular position difference φ, realized by a weak laser beam, is needed for the calculation. Figure 8(a) shows the angular motion analysis for an $N=20$ particle cluster with a constant value of $\varphi=(5.9\pm1.6)°$. Most of the time the cluster rotates as a whole, but there are two events when the shells decouple and intershell rotation occurs. This finding ensures that the applied torque is high enough to drive the cluster to the transition from complete cluster rotation to intershell rotation. The results for $U_\star$ are plotted in Fig. 8(b). For the first half of the sequence shown, where no intershell rotation occurs, $U_\star$ hardly varies and the average $U_\star=0.52\times10^{-18}\ \mathrm{J}=1.9\times10^{-2}E_0$ can be taken as the barrier height. In the second half, $U_\star$ fluctuates strongly, because of the two events of differential rotation. It should be noted here that the experimental value for the intershell rotation barrier is orders of magnitude larger than that predicted for an ideal $N=20$ cluster with Coulomb interaction.[3] The very small theoretical value is based on the ideality of the polygonal structure of the cluster rings. As demonstrated below, nonidealities can modify the intershell barrier dramatically.

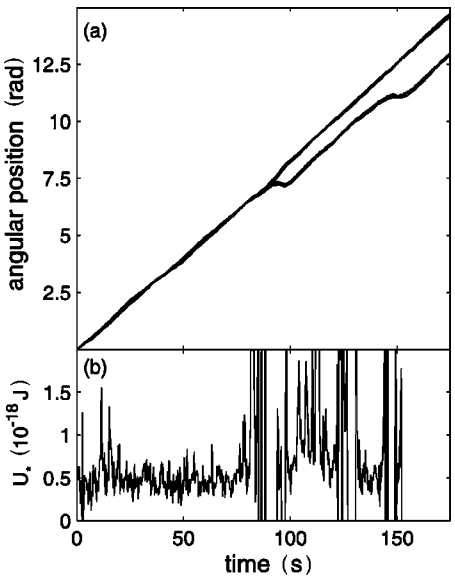

FIG. 8. Relative angular position for 20 particles with weak laser drive (a) and calculated intershell rotation barrier height (b).

The determination of the intershell rotation barrier height for the $N=19$ (1,6,12) cluster cannot be performed in the same way since, before intershell rotation occurs, the structure of the cluster changes. It is therefore only possible to give a minimum value for the intershell barrier $U_\star$. From a similar procedure the intershell rotation barrier for the $N=19$ cluster is found to be $U_\star>0.88\times10^{-18}\ \mathrm{J}=3.2\times10^{-2}E_0$. The theoretical value for pure Coulomb interaction is $U_\star=3.14\times10^{-2}E_0$, for comparison.[3] Obviously, the influence of nonidealities is much smaller for the $N=19$ cluster due to the high symmetry of the cluster structure.

V. MONTE CARLO SIMULATIONS

In this section, the structural transition of the $N=19$ cluster and the intershell rotation barrier will be analyzed by Monte Carlo (MC) simulations under the experimental conditions. The parameters for the simulation, like particle charge, shielding length, and confining potential, were taken from the experiment.

First, the energy barrier for the structural (1,6,12) $\rightarrow$(1,7,11) transition is analyzed. In order to do so, one particle is kept at a fixed position in the simulation and the other

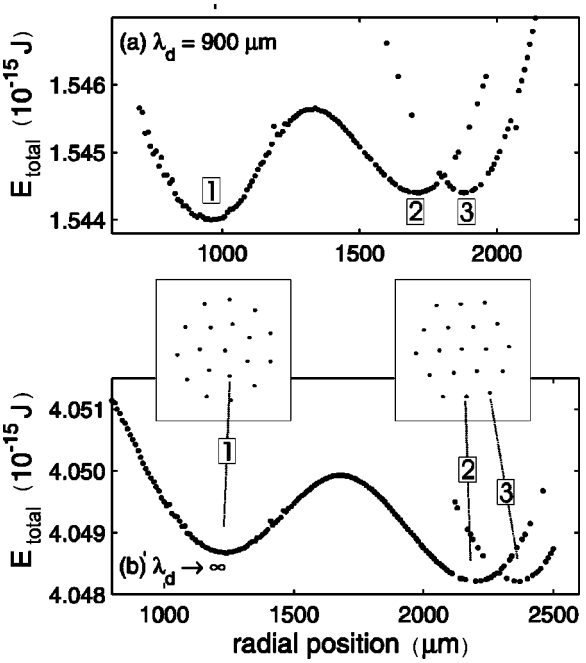

FIG. 9. Simulated total energy $E_{\text{total}}=E_C+E_p$ for a screened (a) and a pure Coulomb system (b) versus radial position of the fixed particle.

particles are left free to adjust their positions. The fixed particle is then moved radially outward. For each radial position the cluster energy is averaged over 10^5 MC steps after 4×10^5 MC steps for equilibration. During the simulation it is ensured that the inner ring contains 6 particles without counting the fixed particle. Figure 9 shows the total energy of the $N=19$ cluster as a function of the radial position of the fixed particle for the shielded case ($\lambda_D=900$ μm) and, for comparison, the Coulomb case ($\lambda_D\rightarrow\infty$). There are three local minima (labeled 1, 2, and 3) that can be assigned to the three stable configurations of the $N=19$ cluster.

When the fixed particle is close to the inner minimum (1) the cluster is in the (1,7,11) structure, since 6 additional particles are in the inner shell. When the fixed particle is in one of the outer minima (2 or 3), the cluster is in the (1,6,12) structure. As the (1,6,12) cluster has a strongly hexagonal ordered structure, the outer ring is a sixfold polygon, although it contains 12 particles. That means that the fixed particle can represent either an edge of the outer hexagon (assigned to minimum 3) or the center of a side of the hexagon (minimum 2), resulting in an alternating radial coordinate (see thumbnail plots in Fig. 9). This explains the two branches of simulated energies at large radius in Fig. 9. The absolute energies calculated from the simulations are in excellent agreement with the experimental data, as well as for the total, potential, and Coulomb energy.

According to the depth of the potential wells, in the Coulomb case [Fig. 9(b)] the (1,6,12) structure is preferred, while in the shielded case [Fig. 9(a)] the (1,7,11) arrangement is more stable. A similar behavior was found recently in Ref. 18. In the shielded case, the two energy levels differ by about 4×10^{-19} J$=1.45\times10^{-2}E_0$. They are separated by an energy barrier of $\Delta E=1.2\times10^{-18}$ J$=4.4\times10^{-2}E_0$. So the (1,6,12) cluster needs an energy of ΔE to make a transition to the (1,7,11) cluster.

In the second step, the energy barrier height of the intershell rotation is calculated for $N=20$ and $N=19$ in the (1,6,12) and (1,7,11) structures with shielding (see Fig. 10). The following procedure has been used in calculating the intershell rotation barrier. After equilibration of the whole system all particles of the inner shell are fixed. Then the angular position of one particle in the outer ring is fixed, too, and rotated around the inner shell, thereby calculating the energy for each angular position of the outer particle. This procedure phenomenologically accounts for the fact that, in the experiment, the shells are not perfect due to small differences in dust size and dust charge. A fixed inner shell may then account for the experimental nonideality. The results of this simulation are listed in Table I.

With fixed core, it is found that the intershell rotation barrier of the sixfold (1,6,12) cluster $U_\star=6.0\times10^{-2}E_0$ with shielding is about a factor of 2 larger than for the Coulomb case $U_\star=3.2\times10^{-2}E_0$ (which is very close to the case of the ideal cluster[3] with $U_\star=3.14\times10^{-2}E_0$). The barriers for the (1,7,11) and (1,7,12) clusters with their broken symmetry are smaller by about factors of 3 to 5 with respect to the (1,6,12) structure, but orders of magnitude larger than for the theoretical Coulomb case $U_\star(1,7,12)=2.01\times10^{-11}E_0$.[3]

From the simulation the barrier is found to be periodic in $2\pi/N_2$, where N_2 is the number of particles in the outer shell. This value has been used in the experimental determination of the intershell barrier. The experimental values lie in the range of the values obtained from the simulation. The range in the simulation is found from different simulation runs with different degrees of nonideality of the inner ring. The value obtained for the intershell barrier strongly depends on the exact structure of the fixed inner ring. It is therefore reasonable to assume that the difference between the experimental value and the result for the ideal case[3] is indeed due to a nonideality of the experimental dust cluster.

TABLE I. Comparison of experimental values and Monte Carlo simulation results for the intershell barrier $U_\star$ and periodicity $\varphi_\star$.

Configuration	Simulation			Experiment	
	$U_\star$		$\varphi_\star$	$U_\star$	
	(10^{-18} J)	($10^{-2}E_0$)	(rad)	(10^{-18} J)	($10^{-2}E_0$)
(1,6,12)	1.65 ± 0.02	6.0 ± 0.09	$2\pi/12$	>0.88	>3.2
(1,7,11)	0.52 ± 0.32[a]	1.9 ± 1.2[a]	$2\pi/11$		
(1,7,12)	0.33 ± 0.32[a]	1.3 ± 1.2[a]	$2\pi/12$	0.52	1.9

[a]The large range is due to different runs with different degrees of nonideality in the inner ring.

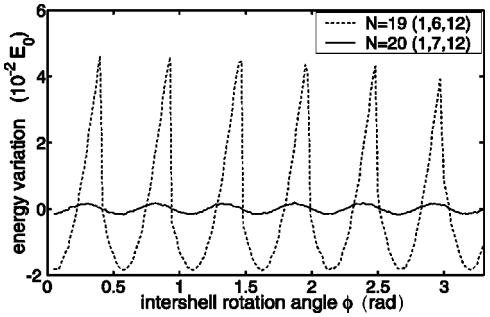

FIG. 10. Simulated relative total energy variation as a function of φ of (a) a (1,6,12) cluster and (b) a (1,7,12) cluster with fixed core.

We are now able to explain the complex behavior of the $N=19$ cluster with applied laser torque. The intershell rotation barrier for the (1,6,12) structure ($U_\star = 0.06E_0$) is indeed larger than the energy barrier for a structural transition, $\Delta E = 0.044E_0$. Therefore, it is not favorable for this structure to exhibit an intershell rotation, but rather to perform a transition into the (1,7,11) structure. There, the intershell rotation barrier $U_\star = 0.002E_0$ is much lower than the configuration barrier, allowing for the observed intershell rotation.

When comparing this to the case of pure Coulomb interaction, the intershell barrier $U_\star = 0.03E_0$ is lower than the configuration barrier of $0.06E_0$ (see Fig. 9), which favors the intershell rotation over the structural transition, in contrast to the experimental results.

The unavoidable effect of shielding in dusty plasmas therefore provides basic changes in the least unstable modes of these clusters.

VI. SUMMARY

We have presented experiments on finite Coulomb clusters in dusty plasmas. We have demonstrated the direct excitation of intershell rotations in these systems by applying a variable torque on the cluster by means of two laser beams. Special attention was paid to the pair of $N=19$ and $N=20$ particles, where the intershell barrier has been determined. The experimental values have been found in good agreement with additional Monte Carlo simulations of the rotation barrier, taking into account effects of nonideality. The $N=19$ cluster in the (1,6,12) configuration exhibits a structural transition into the (1,7,11) structure, which is energetically favored over intershell rotation in the shielded system, in contrast to the case of pure Coulomb interaction.

ACKNOWLEDGMENT

This work is part of the INTAS-RFBR cooperation and was supported under the contract ''Ordered Structures and Coulomb Crystallization in Dusty Plasmas,'' Proposal Number 775.

[1] J. J. Thomson, Philos. Mag. **39**, 236 (1904).
[2] V. M. Bedanov and F. Peeters, Phys. Rev. B **49**, 2667 (1994).
[3] V. A. Schweigert and F. Peeters, Phys. Rev. B **51**, 7700 (1995).
[4] P. Leiderer, W. Ebner, and V. B. Shikin, Surf. Sci. **113**, 405 (1987).
[5] *Nanostructure Physics and Fabrication*, edited by M. A. Reed and W. P. Kirk (Academic, Boston, 1989).
[6] J. E. Hug, F. van Swol, and C. F. Zukoski, Langmuir **11**, 111 (1995).
[7] S. Neser, T. Palberg, C. Blechinger, and P. Leiderer, Prog. Colloid Polym. Sci. **104**, 194 (1997).
[8] W.-T. Juan, Z.-H. Huang, J.-W. Hsu, Y.-J. Lai, and L. I, Phys. Rev. E **58**, 6947 (1998).
[9] J. H. Chu and L. I, Phys. Rev. Lett. **72**, 4009 (1994).
[10] H. Thomas, G. E. Morfill, V. Demmel, J. Goree, B. Feuerbacher, and D. Möhlmann, Phys. Rev. Lett. **73**, 652 (1994).
[11] Y. Hayashi and K. Tachibana, Jpn. J. Appl. Phys., Part 2 **33**, L804 (1994).
[12] A. Melzer, T. Trottenberg, and A. Piel, Phys. Lett. A **191**, 301 (1994).
[13] A. Homann, A. Melzer, S. Peters, R. Madani, and A. Piel, Phys. Rev. E **56**, 7138 (1997).
[14] A. Homann, A. Melzer, R. Madani, and A. Piel, Phys. Lett. A **242**, 173 (1998).
[15] A. Homann, A. Melzer, and A. Piel, Phys. Rev. E **59**, 3835 (1999).
[16] K. Takahashi, T. Oishi, K. Shimomai, Y. Hayashi, and S. Nishino, Phys. Rev. E **58**, 7805 (1998).
[17] A. Melzer, V. A. Schweigert, and A. Piel, Phys. Rev. Lett. **83**, 3194 (1999).
[18] Y.-L. Lai and L. I, Phys. Rev. E **60**, 4743 (1999).
[19] U. Konopka, L. Ratke, and H. M. Thomas, Phys. Rev. Lett. **79**, 1269 (1997).
[20] L. Candido, J.-P. Rino, N. Studart, and F. Peeters, J. Phys.: Condens. Matter **10**, 11 627 (1998).
[21] T. Trottenberg, A. Melzer, and A. Piel, Plasma Sources Sci. Technol. **4**, 450 (1995).
[22] S. Peters, A. Homann, A. Melzer, and A. Piel, Phys. Lett. A **223**, 389 (1996).
[23] M. Zuzic, H. Thomas, and G. E. Morfill, J. Vac. Sci. Technol. A **14**, 496 (1996).
[24] J. B. Pieper and J. Goree, Phys. Rev. Lett. **77**, 3137 (1996).
[25] H. Schollmeyer, A. Melzer, A. Homann, and A. Piel, Phys. Plasmas **6**, 2693 (1999).